Calibration of a simple and a complex model of global marine biogeochemistry

Iris Kriest[1]

[1]GEOMAR Helmholtz-Zentrum für Ozeanforschung Kiel, Düsternbrooker Weg 20, D-24105 Kiel, Germany

Correspondence to: Iris Kriest (ikriest@geomar.de)

Abstract.

The assessment of the ocean biota's role in climate climate change is often carried out with global biogeochemical ocean models that contain many components, and involve a high level of parametric uncertainty. Examination the models' fit to climatologies of inorganic tracers, after the models have been spun up to steady state, is a common, but computationally expensive procedure to assess model performance and reliability. Using new tools that have become available for global model assessment and calibration in steady state, this paper examines two different model types - a complex seven-component model (MOPS), and a very simple two-component model (RetroMOPS) - for their fit to dissolved quantities. Before comparing the models, a subset of their biogeochemical parameters has been optimised against annual mean nutrients and oxygen. Both model types fit the observations almost equally well. The simple model, which contains only nutrients and dissolved organic phosphorus (DOP), is sensitive to the parameterisation of DOP production and decay. The spatio-temporal decoupling of nitrogen and oxygen, and processes involved in their uptake and release, renders oxygen and nitrate valuable tracers for model calibration. In addition, the non-conservative nature of these tracers (with respect to their upper boundary condition) introduces the global bias as a useful additional constraint on model parameters. Dissolved organic phosphorous at the surface behaves antagonistically to phosphate, and suggests that observations of this tracer - although difficult to measure - may be an important asset for model calibration.

1 Introduction

Global biogeochemical ocean models are now routinely used to assess the ocean biota's role in climate change. Although these models have become ever more complex with respect to the number of biogeochemical tracers they contain, they are often calibrated only against a subset of their components, mostly nutrients, oxygen, and components of the carbon cycle (e.g. Bacastow and Maier-Reimer, 1991; Ilyina et al., 2013; Cocco et al., 2013; Cabre et al., 2015).

There has been an intensive discussion about the necessary level of marine ecosystem model complexity, mostly on a theoretical basis, or in a local or regional context (e.g., Anderson, 2005; Le Quere, 2006; Flynn, 2006; Anderson, 2006; Leles et al., 2016; Shimoda and Arhonditsis, 2016). It remains an open question whether additional complexity is of advantage for representing biogeochemical processes and tracers on a global scale (i.e., for processes acting on rather long time and large space scales; e.g., Kriest et al., 2010, 2012; Cabre et al., 2015). A thorough and dense scan of the parameter space would

be required for a fair assessment of the virtues of models of different complexity. Such a scan usually requires many model evaluations, which, given long equilibration time scales of coupled global models (Khatiwala, 2008; Wunsch and Heimbach, 2008; Primeau and Deleersnijder, 2009; Siberlin and Wunsch, 2011), is difficult to carry out. For assessment of only surface properties and processes a short model spinup may be sufficient; however, on a global scale, many centuries to millennia
5   of coupled model simulations are necessary, in order to remove the drift in biogeochemical tracer fields and fit to observed properties (Kriest and Oschlies, 2015; Seferian et al., 2016).

Only recently tools have become available that allow for a reduction in simulation times, such as the Transport Matrix Method (TMM, Khatiwala et al., 2005), Newton's method, which requires the inverse of the Jacobian (Kwon and Primeau, 2006, 2008), matrix-free Newton-Krylov (MFNK, Khatiwala, 2008; Li and Primeau, 2008), or surrogate-based optimisation
10 (Priess et al., 2013). The gain in computational efficiency resulting from these methods can then be used for a systematic calibration of global biogeochemical models. For example, Kwon and Primeau (2006, 2008) used global climatological data sets of phosphate, inorganic carbon, and alkalinity to calibrate a simple global biogeochemical model. The misfit between observed and simulated phosphate was used by DeVries et al. (2014) to calibrate parameters related to particle properties in a simple two-component, nutrient-restoring model. In a similar approach Holzer et al. (2014) optimised parameters for opal
15 production and dissolution against observed silicate. Letscher et al. (2015) switched between a complex and a simple model of ocean biogeochemistry to estimate production and decay rates of dissolved organic phosphorus on a global scale.

All these biogeochemical models employed in global parameter estimates were of a low level of biogeochemical complexity. One reason for this restriction might be the large number of tracers in more complex models, which increases simulation time. Another problem is associated with the variety of time scales associated with more complex models. Piwonski and Slawig
20 (2016) used MFNK to evaluate the steady state of simple and complex biogeochemical models. They noted that "[...] for more complex models the Newton method requires more attention to solver parameter settings [...]" (Piwonski and Slawig, 2016), which may be related to the highly nonlinear structure of these models. The nonlinearity, and the large number of parameters, also complicates their simultaneous optimisation (Ward et al., 2010). On a global scale, these problems are amplified by the sparsity of observations of organism groups, particularly of higher trophic levels. Observations of dissolved inorganic con-
25 stituents, on the other hand, are much more frequent, and therefore provide more information on the spatio-temporal variability of these tracers.

Recently, Kriest et al. (2017) combined the TMM with an estimation of distribution algorithm (Covariance Matrix Adaption Evolution Strategy, CMA-ES), to optimize six biogeochemical parameters of a seven component model against global climatologies of annual mean phosphate, nitrate and oxygen. They showed that annual mean tracer concentrations do not pro-
30 vide much information on parameters related to the dynamic biological processes taking place in the euphotic zone, but that parameters related to larger time- and space scales could be estimated from these observations. To follow up on this, I here investigate if parameters related to oxidant-dependent decay in the mesopelagial are better constrained by this type of misfit function. This is done by replacing four parameters of the optimisation carried out by Kriest et al. (2017) by parameters related oxidant-affinity of remineralisation, and - to account for the possible alterations in fixed nitrogen turnover - by the maximum
35 nitrogen fixation rate.

Given the successful parameter optimisation of simpler models noted above, and also to acknowledge the fact, that these models have been popular and quite successful in global simulations of ocean biogeochemistry, this paper further presents an optimised model, which has been derived from downscaling the seven-component model MOPS (Kriest and Oschlies, 2015; Kriest et al., 2017) to a model that retains only three abiotic dissolved tracers (phosphate, nitrate, and oxygen) and one

5 biotic tracer (dissolved organic phosphorus; DOP). This new model, which I refer to as "RetroMOPS", includes the oxidant-dependency of MOPS, but is otherwise very similar to models applied earlier in global models. In contrast to some of these models (Marchal et al., 1998; Najjar et al., 2007) it assumes no relaxation to observed tracer fields, but simulates changes in surface production fully prognostic, as in Bacastow and Maier-Reimer (1991); Maier-Reimer (1993); Matear and Hirst (2003); Parekh et al. (2005).

10 After a brief presentation of model MOPS (Kriest and Oschlies, 2015), the downscaled model RetroMOPS is introduced, followed by an outline on circulation, optimisation and experimental design (section 2). In section 3 results from optimisation of both MOPS and RetroMOPS are presented and discussed. The paper closes with conclusions drawn from these experiments.

2 Models, experiments, and optimisations

2.1 Model MOPS

15 Model MOPS (Kriest and Oschlies, 2015) is based on phosphorus, and simulates seven compartments. Phosphate, phytoplankton, zooplankton, dissolved organic phosphorus (DOP) and detritus are calculated in units of mmol P m^{-3}. Oxygen is coupled to the P-cycle with a constant stoichiometry given by $R_{-\mathrm{O2:P}}$. Aerobic remineralisation of organic matter follows a saturation curve, with half-saturation constant K_{O2}. Aerobic remineralisation ceases when oxygen declines; at the same time, denitrification takes over, as long as nitrate is available above a defined threshold, DIN_{min}. Like the oxic process, suboxic

20 remineralisation follows a saturation curve for oxidant nitrate, with half-saturation constant K_{DIN}. MOPS does not explicitly resolve the different oxidation states of inorganic nitrogen (nitrite, N$_2$O, ammonium), but assumes immediate coupling of the the different processes involved in nitrate reduction, the end-product being dinitrogen (see also Paulmier et al., 2009; Kriest and Oschlies, 2015). All organic components are characterised by a constant N:P stoichiometry of $d = 16$. Loss of fixed nitrogen is balanced by a simple parameterisation of nitrogen fixation by cyanobacteria, which relaxes the nitrate-to-phosphate ratio to d

25 with a time constant, μ_{NFix}^*. Detritus sinks with a vertically increasing sinking speed: $w = a z$. Assuming a constant degradation rate r, in equilibrium this would result in a particle flux curve given by $F(z) \propto z^{-b}$, with $b = r/a$. For better comparison with values of b derived from observations (e.g. Martin et al., 1987; Van Mooy et al., 2002; Buesseler et al., 2007), and with the simpler model RetroMOPS (see below), a is expressed in terms of b (assuming constant, nominal $r = 0.05$ d^{-1}). A fraction of detritus deposited at the sea floor (at the bottom of the deepest vertical box) is buried instantaneously in some hypothetical

30 sediment. Non-buried detritus is resuspended into the water column, where it is treated as regular detritus. The phosphorus budget is closed on an annual time scale through resupply via river runoff. More details about the biogeochemical model and parameters can be found in Kriest and Oschlies (2013) and Kriest and Oschlies (2015).

2.2 Model RetroMOPS

MOPS' structure has been simplified by skipping the explicit simulation of phytoplankton, zooplankton, and detritus. The remaining equations of, and functional relationships between, phosphate, nitrate, oxygen and DOP have been parameterised similar to MOPS. Because the downscaled model resembles so many features of earlier biogeochemical models simulated in a global context (e.g., Bacastow and Maier-Reimer, 1991; Maier-Reimer, 1993; Matear and Hirst, 2003), but keeps the oxidant dependency of MOPS, the model is named "RetroMOPS".

2.2.1 Primary production

Like MOPS, RetroMOPS calculates primary production only in the euphotic zone, which, in the current configuration, is confined to the upper two numerical layers ($k_{\mathrm{EZ}} = 2$, $z = 0-120$ m). Phytoplankton is parameterised with a constant concentration of $\overline{PHY} = 0.02$ mmol P m^{-3}, which is the mean phytoplankton concentration in the upper 120 m of two optimised model setups MOPS$^{\mathrm{oS}}$ and MOPS$^{\mathrm{oD}}$ (see below). Using this constant phytoplankton concentration RetroMOPS calculates light- and nutrient dependent primary production P in each layer k as:

$$P(k) = \begin{cases} \mu_{\mathrm{PHY}} \, \overline{PHY} \min \left(f(I(k)), \frac{L(k)}{K_{\mathrm{PHY}} + L(k)} \right) & : \quad k \leq k_{\mathrm{EZ}} \\ 0 & : \quad k > k_{\mathrm{EZ}} \end{cases} \tag{1}$$

where $f(I(k))$ defines light-limitation, μ_{PHY} is the temperature-dependent maximum growth rate of phytoplankton, and L determines the limiting nutrient: $L(k) = \min(\mathrm{PO}_4(k), \mathrm{DIN}(k)/d)$ (see Kriest and Oschlies, 2015, for more details).

2.2.2 The fate of primary production: Export, DOP production and remineralisation

Instead of resolving heterotrophic processes (zooplankton grazing, excretion and egestion) at the sea surface explicitly, in RetroMOPS a fraction σ_{DOP} of organic matter fixed photosynthetically is immediately released as dissolved organic phosphorous, DOP. DOP then decays to phosphate and nitrate with a constant rate λ_{DOP}. To allow for a potential, fast recycling loop at the surface, RetroMOPS parameterises an additional decay rate, λ_{sDOP}, that affects DOP only in the first two layers. The remaining fraction of production, $1 - \sigma_{\mathrm{DOP}}$, of each layer in the euphotic zone is exported to the layers below, where it immediately remineralises to nutrients, following a power-law of depth. The discretised form for flux F into box j from all (surface) source layers k, with $1 \leq k \leq k_{\mathrm{EZ}}$ is then given by:

$$F(j) = \sum_{k=1}^{k=k_{\mathrm{EZ}}} P(k)(1 - \sigma_{\mathrm{DOP}}) \Delta z(k) \left(\frac{z(j)}{z(j+1)} \right)^{-b} \qquad \text{for} \quad j > k \,, \tag{2}$$

where $\Delta z(k)$ denotes the thickness of a numerical (source) layer, and $z(j)$ is the depth of the upper boundary of layer j. The flux divergence, $D = \mathrm{d}F/\mathrm{d}z$, for any box j in discretised form is defined by

$$D(j) = \frac{F(j-1) - F(j)}{\Delta z(j)} \tag{3}$$

Neglecting oxidant dependency of decay, the entire flux divergence $D(j)$ would be released as phosphate and nitrate, with
5   equivalent oxidant consumption. It is, however, possible that oxidants become depleted at some location. Earlier models in this case continued the degradation of organic matter, thereby implicitly assuming unspecified oxidants (e.g., Marchal et al., 1998; Matear and Hirst, 2003; Najjar et al., 2007; Kriest et al., 2010, 2012). In contrast, RetroMOPS, like MOPS, accounts for suppression of remineralisation (oxic/suboxic) in the absence of sufficient oxidants, by assuming saturation curves for the limitation by either oxygen or nitrate. The amount of organic matter available for oxidation is given by the decay of dissolved
10   organic matter, $\lambda_{\mathrm{DOP}} DOP$, and by the flux divergence, $D(j)$ (Eqn. 3). The discretised flux divergence, that can actually be remineralised to phosphate and nitrate with available oxidants (oxygen and/or nitrate), $D^{\mathrm{eff}}(j)$, is then determined by

$$D^{\mathrm{eff}}(j) = D(j)\,(s_{\mathrm{O2}}(j) + s_{\mathrm{DIN}}(j)) \qquad , \tag{4}$$

where $s_{\mathrm{O2}}(j)$ and $s_{\mathrm{DIN}}(j)$ represent the oxidant limitation terms, as detailed in Kriest and Oschlies (2015, Equations 15-27). The remaining flux divergence that cannot be remineralised under the given concentrations of oxidants is added as additional
15   flux divergence to the layer below:

$$D(j+1) \quad = \quad D(j+1) + (D(j) - D^{\mathrm{eff}}(j))\,\frac{\Delta z(j)}{\Delta z(j+1)} \tag{5}$$

where again $D^{\mathrm{eff}}(j+1)$ is evaluated. In the bottom layer the remaining flux that has not been remineralised in the water column eventually enters the sediment.

2.2.3 Benthic exchanges

20   Models that implicitly assume unspecified oxidants often prescribe a zero boundary flux, i.e. all organic matter in the last bottom box is degraded instantaneously (e.g., Marchal et al., 1998; Matear and Hirst, 2003; Najjar et al., 2007; Yool et al., 2011). Both MOPS and RetroMOPS have to take "leftover" organic matter flux into account, that arrives undegraded at the sea floor because of incomplete remineralisation in the water column. The explicit detritus compartment in MOPS allows for only partial burial at the sea floor, which may result in detritus accumulation in the deepest model box (see Kriest and Oschlies,
25   2013). Because there is no such detritus compartment in RetroMOPS, all flux arriving at the sea floor is buried immediately. Therefore, MOPS and RetroMOPS differ with respect to their lower boundary condition.

2.2.4 Nitrogen fixation

In RetroMOPS and MOPS nitrogen fixation balances the simulated loss of fixed nitrogen via denitrification. Both models do not explicitly simulate cyanobacteria, but assume zero net growth of these organisms, parameterised as an immediate release of fixed nitrogen as nitrate:

$$
S_{DIN}^{NFix}(k) = \begin{cases} \mu_{\text{NFix}}^{*} \, f_1(\text{T}(k)) \, f_2(\text{DIN}(k), \text{PO}_4(k)) & : \quad k \leq k_{\text{EZ}} \\ 0 & : \quad k > k_{\text{EZ}} \end{cases} \tag{6}
$$

f_1 parameterises the temperature dependence of nitrogen fixation with a second order polynomial approximation of the function by Breitbarth et al. (2007). f_2 regulates the relaxation of the nitrate:phosphate ratio towards the global observed stoichiometric ratio of $d = 16$. μ_{NFix}^{*} is the maximum nitrogen fixation of the parameterized cyanobacteria population (mmol N m^{-3}d^{-1}; see Kriest and Oschlies, 2015, for more details).

2.2.5 Source-minus-sinks

Combining the above mentioned processes and interactions, the time rate of change for phosphate, nitrate, oxygen, and DOP due to biogeochemical processes are

$$
S^{\text{PO4}}(k) = -P(k) + \lambda_{\text{sDOP}} \, \text{DOP} + [D(k) + \lambda_{\text{DOP}} \, \text{DOP}(k)] \, [s_{\text{O2}}(k) + s_{\text{DIN}}(k)] \tag{7}
$$

$$
S^{\text{DOP}}(k) = \sigma_{DOP} \, P(k) - \lambda_{\text{sDOP}} \, \text{DOP} - \lambda_{\text{DOP}} \, \text{DOP}(k) \, [s_{\text{O2}}(k) + s_{\text{DIN}}(k)] \tag{8}
$$

$$
S^{\text{O2}}(k) = R_{-O2:P} \, P(k) - R_{-O2:P} \, \lambda_{\text{sDOP}} \, \text{DOP} - R_{-O2:P} \, [D(k) + \lambda_{\text{DOP}} \, \text{DOP}^{*}] \, s_{\text{O2}}(k) \tag{9}
$$

$$
S^{\text{DIN}}(k) = -d \, P(k) + S_{DIN}^{NFix}(k) + d \, \lambda_{\text{sDOP}} \, \text{DOP} + [D(k) + \lambda_{\text{DOP}} \, \text{DOP}] \, [s_{\text{O2}}(k) \, d - s_{\text{DIN}}(k) \, R_{-\text{DIN:P}}] \tag{10}
$$

Summarising, RetroMOPS is similar to model "N-DOP" of Kriest et al. (2010, 2012), to the phosphorus component of the model presented by Parekh et al. (2005), or to the models presented by Bacastow and Maier-Reimer (1991) and Maier-Reimer (1993), the exception being details of primary production at the sea surface, and the explicit parameterisation of oxidant-dependent remineralisation. By assuming constant cyanobacteria biomass, and a relaxation of the nitrate:phosphate ratio via immediate release of fixed nitrogen, its parameterisation of nitrogen fixation is similar to the one described by Maier-Reimer et al. (2005) and Ilyina et al. (2013).

2.3 Circulation and physical transport

All model simulations apply the Transport Matrix Method (TMM; Khatiwala, 2007, `github.com/samarkhatiwala/tmm`) for tracer transport, with monthly mean transport matrices (TMs) derived from a 2.8° global configuration of the MIT ocean model, with 15 levels in the vertical (Marshall et al., 1997). Using this efficient offline approach, a time step length of 1/2 day for tracer transport and 1/16 day for biogeochemical interactions, simulation of 3000 years requires about 0.5-1.5 hrs on

4 nodes (24 core Intel Xeon Ivybridge) at a High Performance Computing Centre (`www.hlrn.de`). After 3000 years most tracers have approached steady state. The last year is used for model analysis and evaluation of the misfit function.

2.4 Optimisation algorithm

Optimisation of parameters is carried out using an Estimation of Distribution Algorithm, namely the Covariance Matrix Adaption Evolution Strategy (CMA-ES; Hansen and Ostermeier, 2001; Hansen, 2006). The application of this algorithm to the coupled biogeochemistry-TMM framework has shown good performance with respect to quality and efficiency (in terms of function evaluations), and is described only briefly below. More details about the algorithm, its setup and coupling to the global biogeochemical model can be found in Kriest et al. (2017).

Let n be the number of biogeochemical parameters to be estimated. In each iteration ("generation") the algorithm defines a population of λ individuals (biogeochemical parameter vectors of length n), with $\lambda = 10$ (derived from the default parameter $\lambda = 4 + 3\ln(n)$, Hansen and Ostermeier, 2001). The candidate vectors are sampled from a multi-variate normal-distribution, which generalizes the usual normal distribution, also known as Gaussian distribution, from $\mathbb{R}$ to the vector space $\mathbb{R}^n$.

Following the simulation of these λ individual model setups to steady state (3000 years), the misfit function is evaluated, and information of the current, as well as previous generations is used to update the probability distribution in $\mathbb{R}^n$ such that the likelihood to sample good solutions increases. Usually, the realisation of the probability distribution update ensures that information of former solutions fades out slowly, resisting for several iterations. Therefore, the population (the number of model simulations per generation) in CMA-ES is smaller, and of less computational demand, than in classical evolutionary algorithms. Nevertheless, CMA-ES can still, to a certain degree, perform well with misfit functions characterised by a rough topography (Kriest et al., 2017).

2.5 Misfit function

As in Kriest et al. (2017) the misfit to observations J is defined as the root-mean-square error RMSE between simulated and observed annual mean phosphate, nitrate, and oxygen concentrations (Garcia et al., 2006a, b), mapped onto the three-dimensional model geometry. Deviations between model and observations are weighted by the volume of each individual grid box, V_i, expressed as fraction of total ocean volume, V_T. The resulting sum of weighted deviations is then normalised by the global mean concentration of the respective observed tracer:

$$J = \sum_{j=1}^{3} J(j) \frac{1}{\overline{o_j}} = \sum_{j=1}^{3} \sqrt{\sum_{i=1}^{N} (m_{i,j} - o_{i,j})^2 \frac{V_i}{V_T}} \tag{11}$$

$j = 1, 2, 3$ indicates the tracer type and $i = 1, ..., N$ are the model locations for $N = 52749$ model grid boxes. $\overline{o_j}$ is the global average observed concentration of the respective tracer. $m_{i,j}$ and $o_{i,j}$ are model and observations, respectively. By weighting each individual misfit with volume, J serves more as a long time-scale geochemical estimator, in contrast to a misfit function that e.g. focuses on (rather fast) turnover in the surface layer, or resolves the seasonal cycle.

2.6 Optimisation of MOPS

Building upon the optimisation of mostly surface-related parameters presented in Kriest et al. (2017, "OBS-NARROW", here-after referred to as MOPS$^{\mathrm{oS}}$), optimisation MOPS $^{\mathrm{oD}}$ presented here aims at calibrating parameters related to processes that directly affect the oxidants nitrate and oxygen in subsurface layers. In MOPS $^{\mathrm{oD}}$ the optimal parameters of MOPS$^{\mathrm{oS}}$ for light
5 and nutrient affinity of phytoplankton, zooplankton grazing and its mortality are retained, and parameters relevant for deep aerobic and anaerobic remineralisation are subject to change during optimisation (Table 1).

Parameter K_{O2} determines the affinity of the aerobic remineralisation to oxygen, and the gradual transition from this process to denitrification (see Eqns. 15 and 20 of Kriest and Oschlies, 2015). K_{DIN} determines the affinity of denitrification to nitrate. Parameter $DIN\mathrm{min}$ defines the lower threshold for the onset of denitrification. MOPS$^{\mathrm{oD}}$ also optimises the maximum rate
10 of nitrogen fixation, μ^*_{NFix}, which balances fixed nitrogen loss. The fifth and sixth parameter to be estimated are the oxygen requirement per mole phosphorus remineralised, $R_{-O2:P}$, and the flux (or remineralisation) length scale, b.

To investigate the influence of observations entering the misfit function, MOPS$^{\mathrm{oD}}$ is repeated with a reduced data set, that excludes the eastern equatorial Pacific (east of $140°$W, between $10°$S and $10°$N) from the misfit function. This optimisation is named MOPS$^{\mathrm{oD}}_*$. In the following, results from the optimised models MOPS$^{\mathrm{oS}}$, MOPS$^{\mathrm{oD}}$ and MOPS$^{\mathrm{oD}}_*$ are compared to a
15 reference experiment, MOPS$^{\mathrm{r}}$, which represents a "hand-tuned", a priori setup of this model.

2.7 Optimisation of RetroMOPS

In model RetroMOPS processes such as grazing of phytoplankton, and its subsequent release of organic or inorganic phosphorus are parameterised via a single component, DOP. Because DOP production and decay regulate the partitioning between sinking and dissolved organic matter, optimisation RetroMOPS$^{\mathrm{o}}$ targets at these parameters, namely σ_{DOP}, λ_{sDOP} and λ_{DOP}.
20 While σ_{DOP}, as parameter that regulates the export ratio, may be more or less well constrained, λ_{sDOP} and λ_{DOP} both include a variety of processes, which may act on time scales of days to years. In a set of nine a priori sensitivity experiments the effect of these parameters on the misfit function is explored by varying λ_{DOP} between 0.18 y^{-1} and 0.72 y^{-1}, and λ_{sDOP} between 0 y^{-1} and 0.36 y^{-1} (see table 2). The results of these sensitivity experiments provide a guidance for upper and lower boundaries of optimisation (table 1). The sensitivity experiment with the lowest misfit ($\lambda_{\mathrm{sDOP}} = 0$, $\lambda_{\mathrm{DOP}} = 0.36$) is used for
25 comparison with the optimised RetroMOPS, and referred to as RetroMOPS$^{\mathrm{r}}$.

The explicit representation of detritus in MOPS may result in considerable numerical diffusion (particularly on coarse vertical grids as used here; see also Kriest and Oschlies, 2011) and thus in a different estimate of optimal b then when applying a direct flux curve, such as in RetroMOPS. Therefore, b is included as fourth parameter to be optimised.

3   Results and discussion

3.1   Optimisation of MOPS

Both $R_{-O2:p}$ and b are constrained very well by the observations, as indicated by a well-defined minimum of the misfit function (Fig. S1), and the narrow, almost gaussian distribution of the best 10% to 1‰ of parameters (Fig. 1, Table 3). The good determination of b by dissolved inorganic tracers is agreement with earlier studies (Kwon and Primeau, 2006; Kriest et al., 2017; Schartau et al., 2016). Parameters related to oxidant-dependent remineralisation approach the lower (K_{O2}) or upper (K_{DIN}, DIN_{min}) boundary, with a rather wide, skewed distribution. The rate for maximum nitrogen fixation shows a slightly skewed distribution, but suggests an overall good estimate of this parameter.

Fixed nitrogen loss and gain depend on parameters for oxidant-dependency of remineralisation: In MOPS[oS], both fluxes are very high (Fig. 2), and outside the observed range (Table 4). Because optimisation MOPS[oD] results in a strongly reduced affinity to, and higher threshold of, nitrate, its pelagic fixed nitrogen loss is almost halved, and now agrees with observed global estimates (Table 4). Further, as a result of reduced denitrification, the nitrate deficit in the eastern equatorial Pacific is smaller; however, at the cost of a small underestimate of observed oxygen in this region (Fig. 3). The latter is a consequence of the now very low half-saturation constant for oxygen uptake (Table 3). Overall, optimisation of parameters related to the oxidant affinity of oxic and suboxic remineralisation leads to a slightly improved fit to tracer concentrations, to $J^* = 98\%$ of that of MOPS[oS] (Table 3), and to a better agreement with observed estimates of global biogeochemical fluxes (Table 4).

Optimisation MOPS[oD] results in a high treshold for the limitation of denitrification, with K_{DIN} and DIN_{min} close to their upper boundaries. The increase protects nitrate from becoming depleted in the upwelling regions, particularly the eastern equatorial Pacific, and resembles results obtained by Moore and Doney (2007): To prevent their model from reproducing unrealistically low nitrate values in this region, they had to impose a threshold of 32 mmol NO_3 m^{-3} for the occurrence of denitrification. An explanation for this requirement of a high nitrate threshold might be found in the representation of the equatorial intermediate current system in coarse resolution models, which can result in spurious zonal oxygen gradients (Dietze and Loeptien, 2013; Getzlaff and Dietze, 2013). It is possible that the optimisation of biogeochemical parameters attempts to ameliorate these effects, which are in fact caused by the parameterisation of physics.

To investigate the impact of this region on the parameter estimate, an additional optimisation was carried out, that applies the same set of parameters to be optimised, but omits the eastern equatorial Pacific from the calculation of the misfit function. This optimisation MOPS$_*^{oD}$ generates a lower threshold of nitrate for the onset of denitrification, and a higher maximum nitrogen fixation rate (Table 3), resulting in slightly enhanced fixed nitrogen turnover, particularly in the eastern equatorial Pacific (Fig. 2). Global fixed nitrogen loss increases by about 20%, towards the upper limit of observed estimates (Table 4). Compared to MOPS[oD] the estimates of K_{DIN} and DIN_{min} become more uncertain with respect to the best 10% to 1‰ individuals, and show an even bimodal distribution (Fig. S2, Table 3). The uncertainty in parameter estimates can be related to the missing data in regions of simulated denitrification. Summarising, although the eastern equatorial Pacific, and potential unresolved processes in simulated circulation, evoke only relatively small effects on some parameter estimates, these nevertheless result in an increase in global fixed nitrogen loss of about 20%.

3.2 Sensitivity of RetroMOPS to DOP production and decay

In RetroMOPS fast DOP recycling leads to the higher primary production, export production, and deep organic particle flux, especially in the equatorial upwelling regions (Fig. 4). While this has only a small effect on vertically or globally averaged phosphate concentrations (Figures 5 and 6), it leads to a a large underestimate of nitrate in the ocean (Figures S4 and 6). The

5 underestimate can be explained by the tight coupling between production, export and denitrification, which leads to higher denitrification and global fixed N-loss (Fig. 4), and thus a larger nitrate deficit (Fig S4) in the eastern equatorial Pacific. This is in agreement with effects hypothesised and investigated by Landolfi et al. (2013).

In the model nitrogen fixation counteracts fixed nitrogen loss through denitrification. In contrast to nitrogen fixation, which is not much affected by DOP turnover rates, global fixed nitrogen loss increases with increasing DOP decay rate (Fig. 4).

10 The imbalance between nitrogen losses and gains suggests that the models even after 3000 years of simulation are not yet in equilibrium. It might be explained by the large spatial scales between regions of fixed nitrogen loss and gain, in conjunction with the slow turnover rates of the biogeochemical processes. The divergence increases with increasing recycling rates, indicating that there is no unique equilibration time scale for one and the same model, but that it depends on biogeochemical parameters associated with sinking and remineralisation of organic matter, as observed earlier (Kriest and Oschlies, 2015). The resulting

15 long spinup times, their dependence on biogeochemical parameters, and the model's nonlinearity during spinup (Kriest and Oschlies, 2015), complicate model calibration and assessment, in addition to those factors already investigated by Seferian et al. (2016).

The effect of DOP recycling on oxygen concentrations differs from its effect on nitrate. With fast recycling DOP is remineralised mostly at its place of production, and does not contribute much to oxygen consumption in deep waters (see also Fig S3).

20 As a consequence, deep oxygen concentrations are high, particularly in the northern North Pacific (Fig. 5), and global average oxygen is overestimated by more than 10% (Fig. 6). Slow DOP recycling, in contrast, leads less organic matter remineralisation in preformed, well-ventilated waters, but more remineralisation in deep waters. This in turn results in an underestimate of global mean oxygen of almost 10% (for $\lambda_{\mathrm{DOP}} = 0.18\,\mathrm{y}^{-1}$ and $\lambda_{\mathrm{DOP}} = 0$), which is somewhat surprising, given that production and export in this scenario are the lowest of all simulations (Fig. 4).

25 Overall, the best fit to observed inorganic tracer concentrations is achieved with moderate DOP recycling (Table 2, Fig. 5). Most likely because of its fixed inventory, phosphate contributes to less than 1/3 of the misfit function, and is quite insensitive to changes in DOP recycling rate (Fig. 6). Nitrate and oxygen play a larger role for model fit, because their inventory can adapt to changing biogeochemistry. The misfit to nitrate and oxygen more or less increases in concert with their bias (Fig. 6). Therefore, these tracers with their flexible inventory provide some very useful constraints on DOP recycling rates.

30 Slow DOP recycling increases DOP concentrations, particularly in the ACC and in the northern North Atlantic (Fig. 5), and simulated concentrations largely exceed the observations (Yoshimura et al., 2007; Raimbault et al., 2008; Torres-Valdes et al., 2009; Letscher and Moore, 2015). Only the simulation with quite fast DOP recycling of $\lambda_{\mathrm{DOP}} = 0.72\,\mathrm{y}^{-1}$ and $\lambda_{\mathrm{sDOP}} = 0.36\,\mathrm{y}^{-1}$ results in reasonable concentrations of DOP - but at the cost of too high phosphate concentrations along these sections, and a too high global misfit (Table 2), a too low nitrate and too high oxygen inventory (Figures 5 and 6).

3.3 Optimisation of RetroMOPS

All four parameters of RetroMOPS[o] are quite well constrained by the observations, as indicated by the narrow, almost gaussian distribution around the optimal parameter (Figures 7, S5, and Table 3). Optimisation reduces the decay rate for surface DOP, λ_{sDOP}, to almost zero, i.e., in RetroMOPS there seems to be no requirement for fast DOP turnover at the surface. The optimal

5 DOP total remineralisation rate is about 0.5 y^{-1}, and the optimal fraction of primary production released as DOP is 73%, resulting in a slightly higher turnover as compared to the reference scenario RetroMOPS[r]. Optimal σ_{DOP} agrees very well with $\sigma = 0.74$ obtained by Kwon and Primeau (2006); however, their optimal DOP decay rate was twice as high (1 y^{-1}).

When optimising a simple biogeochemical model similar to RetroMOPS against observed phosphate, Kwon and Primeau (2006) noted a correlation between DOP production fraction and decay rate, impeding the simultaneous estimation of these

10 parameters. On the contrary, in optimisation RetroMOPS[o] both σ_{DOP} and the DOP decay rates seem to be rather well constrained. An analysis of the different components of the misfit function, similar to Fig. 4 of Kwon and Primeau (2006), helps to resolve this apparent contradiction. For this, in Fig. 8 misfit (J and $J(j)$ of Eqn. 11) and bias of the best 5% of all individual is mapped against σ_{DOP} and DOP decay timescale $\tau = 1/(\lambda_{\mathrm{DOP}} + \lambda_{\mathrm{sDOP}})$.

Note that the analysis depicted in Fig. 8 differs from that of Kwon and Primeau (2006) in several aspects: Firstly, their global

15 biogeochemical model was fully equilibrated (due to their direct evaluation of steady state), whereas simulations of RetroMOPS may still exhibit some drift in nitrogen inventory (see subsection 3.2). Second, Kwon and Primeau (2006) evaluated model sensitivity at $b = 1$, while Fig. 8 displays a region $\pm 5\%$ around optimal b. Thirdly, Fig. 8 maps only the misfit of solutions realised by the optimisation routine, while Kwon and Primeau (2006) analysed the entire parameter space at $b = 1$. Finally, the misfit function applied here is based on three components, with very different properties and associated time scales (see

20 above), which can be of advantage for parameter estimation.

The misfit to phosphate (Fig. 8, lower left panel) shows an elongated valley in the two-dimensional projection on DOP decay timescale τ (years) and DOP production fraction σ_{DOP}, and resembles Fig. 4 of Kwon and Primeau (2006). Indeed, one of the lowest misfits to phosphate is achieved with about the same set of parameters as in Kwon and Primeau (2006), namely $\tau \approx 1$, $\sigma_{\mathrm{DOP}} \approx 0.73$. However, nitrate and oxygen show a different, and, partly, antagonistic, pattern: the best fit to observed nitrate

25 is achieved with rather high values of $\sigma_{\mathrm{DOP}} \approx 0.8$ and τ between about 1-2 years, while the best fit to oxygen is obtained with $\sigma_{\mathrm{DOP}} \approx 0.7$ and $\tau \approx 1.5$ years. The superposition of the different components of the misfit function leads to a unique optimum of $\tau = 2$ ($\lambda_{\mathrm{DOP}} = 0.47$ and $\lambda_{\mathrm{DOP}} = 0.02$) and $\sigma_{\mathrm{DOP}} = 0.73$ (Table 3). Thus, oxygen and nitrate can provide some useful, independent information on these parameters.

As noted above, the advantage of including nitrate and oxygen in the misfit function is that, in contrast to phosphate, the

30 inventory of these tracers may change freely according to model parameterisation. The resulting bias to observations thus adds two important components to the misfit function, both of which are independent: while high DOP turnover (as simulated by low τ) biases nitrate low (Fig. 8, upper mid panel), the same value leads to an overestimate of oxygen (Fig. 8, upper right panel; see also Fig. 6). This behaviour can be explained with the different processes and boundary conditions for the two tracers already noted above: a high DOP turnover leads to higher fluxes and a tighter coupling of production and denitrification in upwelling

waters, causing a nitrate deficit in the model (see above, and Fig S4). On the contrary, it reduces DOP in preformed waters e.g., in the Southern Ocean, thereby decreasing aerobic remineralisation and oxygen consumption in these waters on their passage towards, e.g., the northern North Pacific. The latter process increases oxygen particularly in deep waters (Fig S3).

The optimal $b = 0.98$ of RetroMOPS° is lower than that of MOPS^{oS} and MOPS^{oD}. This may be partially explained with the

5 absence of numerical diffusion of detritus in RetroMOPS. As shown by Kriest and Oschlies (2011), in models that explicitly simulate detritus sinking with an upstream scheme, the assumption of homogenous distribution of detritus in each vertical grid box causes an additional, usually downward transport of detritus. This results in an effective b which is about 10-20% smaller (corresponding to faster sinking) than the nominally prescribed b. Optimisation of MOPS accounts for this additional numerical transport by increasing b (= reducing sinking velocity) by some amount. Therefore, optimal b of MOPS without any influence

10 numerical of diffusion would likely be around 1.1-1.2, i.e. closer to $b = 0.98$ of RetroMOPS°. Considering this effect, optimal b of MOPS^{oD} and, in particular, RetroMOPS° agree with the optimal value of $b = 1$ found by Kwon and Primeau (2006).

Despite its generally lower fluxes, fixed nitrogen loss in the eastern equatorial Pacific is higher in RetroMOPS° than in MOPS^{oD} (Fig. 2), resulting in a nitrate deficit in this region. The deficit is comparable to that of MOPS^{oS}, i.e. of a model simulation with default parameters for oxidant dependent processes (Fig. 3). Likely, the instantaneous remineralisation of

15 sinking material inherent in the direct flux parameterisation of RetroMOPS, which causes a tighter spatial coupling between production, sinking, remineralisation and upwelling. It has been suggested earlier that the production of slowly degradable organic matter above upwelling regions and/or oxygen minimum zones may help to decouple these processes, and avoid a runaway effect of nitrate loss (Landolfi et al., 2013; Dietze and Loeptien, 2013). The very low optimal value for surface DOP turnover λ_{sDOP} found in this study supports this finding.

20 The total misfit to observed dissolved tracer concentrations of RetroMOPS° is only about 4% higher than that of MOPS^{oD}, i.e. RetroMOPS can perform almost as well as MOPS, with respect to annual mean phosphate, nitrate, and oxygen. Simulated biogeochemical fluxes of RetroMOPS° are generally lower than those of MOPS^{oD}, and their horizontal pattern is less pronounced (Fig. 2). This likely arises from the prescribed, constant phytoplankton concentration of RetroMOPS°, which mutes biogeochemical dynamics in productive regions of the high latitudes and upwelling areas. Because RetroMOPS° applies the

25 same parameters as MOPS^{oD} for oxidant-dependent processes, its global fixed nitrogen loss and gain is comparable to that of the more complex model. As for MOPS, optimisation of RetroMOPS against dissolved tracer concentrations improves the fit to global estimates of biogeochemical fluxes (Table 4), and indicates, that these tracers can provide means to calibrate biogeochemical model fluxes on a global scale, even - or especially - for a model as simple as RetroMOPS.

4 Conclusions

30 Optimisation of parameters for oxidant-dependent processes results in a slightly better fit to observed tracers, and in a much better fit to observed estimates of global fixed nitrogen turnover. Omission of the eastern equatorial Pacific from the misfit function results in a slight upward bias of global fixed nitrogen fluxes. It does not, however, fundamentally alter the outcome of optimisation. Model optimisations with different parameterisations of circulation and the equatorial intermediate current system

(e.g., using TMs extracted from the UVic model; Kvale et al., 2017) will help to examine, if a different parameterisation alters the current requirement for very high nitrate threshold of denitrification, that currently helps to prevent nitrate from depletion.

Oxygen and nitrate add important additional constraints on the estimation of biogeochemical parameters. Of particular importance is that, in addition to the spatial information they provide, their flexible inventory introduces the bias as additional information for model calibration. The different time and space scales of processes relevant for their inventory may help to constrain parameters that govern dissolved organic matter production and decay. The effect of these tracers on parameter estimates is of particular importance for models such as RetroMOPS and MOPS, that aim at conserving all oxidants. It may be weaker for models that continue remineralisation even under suboxic and/or low nitrate conditions, thereby implicitly assuming some "hidden" oxidants. In these models it could be useful to track and examine potential oxidant deficits for model evaluation.

The DOP recycling rate affects surface DOP and phosphate concentrations conversely: either the model performs relatively well with respect to DOP. In this case phosphate concentrations are overestimated by the model. If the model performs well with respect to phosphate, it overestimates surface DOP. Observations of DOP as additional constraint on model parameters will help to find out if there is a model solution that fits all tracers simulated in RetroMOPS.

With respect to annual mean tracer concentrations the simple model RetroMOPS can perform almost as well as the more complex model MOPS. Although spatial patterns of fluxes in RetroMOPS are less pronounced, global tracer concentrations, inventories and fluxes are comparable to that of MOPS, and in agreement with observed estimates. This of course may change if our scientific interest and model purpose is directed towards shorter time scales, or surface patterns, for which the misfit function applied provides little information. If focusing on large scale dynamics, however, a simple model such as RetroMOPS or similarly simple models may suffice to represent and analyse much of the biogeochemical dynamics in the ocean.

Acknowledgements. I am very thankful for having met Ernst Maier-Reimer, who pioneered global biogeochemical modeling. In his thoughtful and kind way he taught me to view global ocean biogeochemistry before the background of long time and large space scales. Thank you, Ernst!

This work is a contribution to the DFG-supported project SFB754 and to BMBF joint project PalMod (FKZ 01LP1512A). Parallel supercomputing resources have been provided by the North-German Supercomputing Alliance (HLRN). The author wishes to acknowledge use of the Ferret program of NOAA's Pacific Marine Environmental Laboratory for analysis and graphics in this paper.

References

Anderson, T.: Plankton functional type modelling: running before we can walk?, J. Plankton Res., 27, 1073–1081, 2005.

Anderson, T. R.: Confronting complexity: reply to Le Quere and Flynn, Jour. Plankton Res., 28, 877–878, doi:10.1093/plankt/fbl016, 2006.

Bacastow, R. and Maier-Reimer, E.: Dissolved organic carbon in modeling oceanic new production, Global Biogeochem. Cy., 5, 71–85, 1991.

Breitbarth, E., Oschlies, A., and LaRoche, J.: Physiological constraints on the global distribution of *Trichodesmium* - effect of temperature on diazotrophy, Biogeosciences, 4, 53–61, 2007.

Buesseler, K., Lamborg, C., Boyd, P., Lam, P., Trull, T., Bidigare, R., Bishop, J., Casciotti, K., Dehairs, F., Elskens, M., Honda, M., Karl, D., Siegel, D., Silver, M., Steinberg, D., Valdes, J., Mooy, B. V., and Wilson, S.: Revisiting carbon flux through the ocean's twilight zone, Science, 316, 567–570, 2007.

Cabre, A., Marinov, I., Bernadello, R., and Bianchi, D.: Oxygen minimum zones in the tropical Pacific across CMIP5 models: mean state differences and climate change trends, Biogeosciences, 12, 5429–5454, 2015.

Carr, M.-E., Friedrichs, M., Schmeltz, M., Aitac, M., Antoine, D., Arrigo, K., Asanuma, I., Aumont, O., Barber, R., Behrenfeld, M., Bidigare, R., Buitenhuis, E., Campbell, J., Ciotti, A., Dierssen, H., Dowell, M., Dunne, J., Esaias, W., Gentili, B., Gregg, W., , Groom, S., Hoepffner, N., Ishizaka, J., Kameda, T., Quere, C. L., Lohrenz, S., Marra, J., lino, F. M., Moore, K., Morel, A., Reddy, T., J.Ryan, Scardi, M., T.Smyth, Turpie, K., Tilstone, G., Waters, K., and Yamanaka, Y.: A comparison of global estimates of marine primary production from ocean color, Deep-Sea Res. Pt. II, 53, 741–770, 2006.

Cocco, V., Joos, F., Steinacher, M., Frölicher, T., Bopp, L., Dunne, J., Gehlen, M., Heinze, C., Orr, J., Oschlies, A., Schneider, B., Segschneider, J., and Tjiputra, J.: Oxygen and indicators of stress for marine life in multi-model global warming projections, Biogeosciences, 10, 1849–1868, 2013.

DeVries, T., Liang, J.-H., and Deutsch, C.: A mechanistic particle flux model applied to the oceanic phosphorus cycle, Biogeosciences, 11, 5381–5398, 2014.

Dietze, H. and Loeptien, U.: Revisiting "nutrient trapping" in global coupled biogeochemical ocean circulation models, Global Biogeochem. Cy., 27, 265—284, 2013.

Dunne, J. P., Sarmiento, J. L., and Gnanadesikan, A.: A synthesis of global particle export from the surface ocean and cycling through the ocean interior and on the seafloor, Global Biogeochem. Cy., 21, 2007.

Flynn, K. J.: Reply to Horizons Article 'Plankton functional type modelling: running before we can walk' Anderson (2005): II. Putting trophic functionality into plankton functional types, Jour. Plankton Res., 28, 873–875, doi:10.1093/plankt/fbl015, 2006.

Garcia, H. E., Locarnini, R. A., Boyer, T. P., and Antonov, J. I.: World Ocean Atlas 2005, Vol. 4: Nutrients (phosphate, nitrate, silicate), in: NOAA Atlas NESDIS 64, edited by Levitus, S., U.S. Government Printing Office, Wash.,D.C., 2006a.

Garcia, H. E., Locarnini, R. A., Boyer, T. P., and Antonov, J. I.: World Ocean Atlas 2005, Vol. 3: Dissolved Oxygen, Apparent Oxygen Utilization, and Oxygen Saturation, in: NOAA Atlas NESDIS 63, edited by Levitus, S., U.S. Government Printing Office, Wash.,D.C., 2006b.

Getzlaff, J. and Dietze, H.: Effects of increased isopycnal diffusivity mimicking the unresolved equatorial intermediate current system in an earth system climate model, Geophys. Res. Lett., 40, 2166–2170, 2013.

Hansen, N.: The CMA evolution strategy: a comparing review, in: Towards a new evolutionary computation. Advances on estimation of distribution algorithms, edited by Lozano, J. A., Larranaga, P., Inza, I., and Bengoetxea, E., pp. 75–102, Springer, 2006.

Hansen, N. and Ostermeier, A.: Completely Derandomized Self-Adaptation in Evolution Strategies, Evolutionary Computation, 9, 159–195, 2001.

Holzer, M., Primeau, F., DeVries, T., and Matear, R.: The Southern Ocean silicon trap: Data-constrained estimates of regenerated silicic acid, trapping efficiencies, and global transport paths, Journal Of Geophysical Research, 119, 313–331, doi:10.1002/2013JC009356, 2014.

Honjo, S., Manganini, S. J., Krishfield, R. A., and Francois, R.: Particulate organic carbon fluxes to the ocean interior and factors controlling the biological pump: A synthesis of global sediment trap programs since 1983, Prog. Oceanogr., 76, 217–285, 2008.

Ilyina, T., Six, K., Segschneider, J., Maier-Reimer, E., Li, H., and nez Riboni, I. N.: Global ocean biogeochemistry model HAMOCC: Model architecture and performance as component of the MPI-Earth system model in different CMIP5 experimental realizations, Jour. Adv. Model. Earth Systems, 5, 1–29, 2013.

Khatiwala, S.: A computational framework for simulation of biogeochemical tracers in the ocean, Global Biogeochem. Cy., 21, GB3001, 2007.

Khatiwala, S.: Fast spin up of ocean biogeochemical models using matrix-free Newton-Krylov, Ocean Modell., 23, 121–129, 2008.

Khatiwala, S., Visbeck, M., and Cane, M. A.: Accelerated simulation of passive tracers in ocean circulation models, Ocean Modell., 9, 51–69, 2005.

Kriest, I. and Oschlies, A.: Numerical effects on organic matter sedimentation and remineralization in biogeochemical ocean models, Ocean Modell., 39, 275–283, 2011.

Kriest, I. and Oschlies, A.: Swept under the carpet: The effect of organic matter burial in global biogeochemical ocean models, Biogeosciences Disc., 10, 10 859–10 911, 2013.

Kriest, I. and Oschlies, A.: MOPS-1.0: towards a model for the regulation of the global oceanic nitrogen budget by marine biogeochemical processes, Geosci. Model Dev., 8, 2929–2957, doi:10.5194/gmd-8-2929-2015, www.geosci-model-dev.net/8/2929/2015/, 2015.

Kriest, I., Khatiwala, S., and Oschlies, A.: Towards an assessment of simple global marine biogeochemical models of different complexity, Prog. Oceanogr., 86, 337–360, 2010.

Kriest, I., Oschlies, A., and Khatiwala, S.: Sensitivity analysis of simple global marine biogeochemical models, Global Biogeochem. Cy., 26, 2012.

Kriest, I., , Sauerland, V., Khatiwala, S., Srivastav, A., and Oschlies, A.: Calibrating a global three-dimensional biogeochemical ocean model (MOPS-1.0), Geoscientific Model Development, 10, 127–154, doi:10.5194/gmd-10-127-2017, www.geosci-model-dev.net/10/127/2017/, 2017.

Kvale, K., Khatiwala, S., Dietze, H., Kriest, I., and Oschlies, A.: Evaluation of the Transport Matrix Method for simulation of ocean biogeochemical tracers, Geosci. Model Dev. Discuss., doi:10.5194/gmd-2017-29, 2017.

Kwon, E. Y. and Primeau, F.: Optimization and sensitivity study of a biogeochemistry ocean model using an implicit solver and in situ phosphate data, Global Biogeochem. Cy., 20, 2006.

Kwon, E. Y. and Primeau, F.: Optimization and sensitivity of a global biogeochemistry ocean model using combined in situ DIC, alkalinity, and phosphate data, J. Geophys. Res., 113, 2008.

Landolfi, A., Dietze, H., Koeve, W., and Oschlies, A.: Overlooked runaway feedback in the marine nitrogen cycle: the vicious cycle, Biogeosciences, 10, 1351–1363, 2013.

Le Quere, C.: Reply to Horizons Article 'Plankton functional type modelling: running before we can walk' Anderson (2005): I. Abrupt changes in marine ecosystems?, Jour. Plankton Res., 28, 871–872, doi:10.1093/plankt/fbl014, 2006.

Leles, S., Valentin, J., and Figueiredo, G.: Evaluation of the complexity and performance of marine planktonic trophic models, Annals of the Brazilian Academy of Sciences, 88, 1971–1991, doi:10.1590/0001-3765201620150588, 2016.

Letscher, R. and Moore, J. K.: Preferential remineralization of dissolved organic phosphorus and non-Redfield DOM dynamics in the global ocean: Impacts on marine productivity, nitrogen fixation, and carbon export, Glob. Biogeochem. Cyc., 29, 325–340, doi:doi:10.1002/2014GB004904, 2015.

Letscher, R., Moore, J. K., Teng, Y.-C., and Primeau, F.: Variable C : N : P stoichiometry of dissolved organic matter cycling in the Community Earth System Model, Biogeosciences, 12, 209–221, doi:10.5194/bg-12-209-2015, www.biogeosciences.net/12/209/2015, f2, 2015.

Li, X. and Primeau, F.: A fast Newton–Krylov solver for seasonally varying global ocean biogeochemistry models, Ocean Modell., 23, 13–20, 2008.

Lutz, M., Caldeira, K., Dunbar, R., and Behrenfeld, M. J.: Seasonal rhythms of net primary production and particulate organic carbon flux to depth describe biological pump efficiency in the global ocean, J. Geophys. Res., 113, C10011, 2007.

Maier-Reimer, E.: Geochemical cycles in an ocean general circulation model. Preindustrial tracer distributions, Global Biogeochem. Cy., 7, 645–677, 1993.

Maier-Reimer, E., Kriest, I., Segschneider, J., and Wetzel, P.: The HAMburg Ocean Carbon Cycle Model HAMOCC 5.1 - Technical Description Release 1.1, Reports on Earth System Science 14, Max-Planck-Institute for Meteorology, Hamburg, 2005.

Marchal, O., Stocker, T. F., and Joos, F.: A latitude-depth, circulation-biogeochemical ocean model for paleoclimate studies. Development and sensitivities, Tellus Series B-Chemical And Physical Meteorology, 50, 290–316, 1998.

Marshall, J., Adcroft, A., Hill, C., Perelman, L., and Heisey, C.: A finite-volume, incompressible Navier-Stokes model for studies of the ocean on parallel computers, J. Geophys. Res., 102, 5733–5752, 1997.

Martin, J. H., Knauer, G. A., Karl, D. M., and Broenkow, W. W.: VERTEX: carbon cycling in the Northeast Pacific, Deep-Sea Res., 34, 267–285, 1987.

Matear, R. J. and Hirst, A. C.: Long-term changes in dissolved oxygen concentrations in the ocean caused by protracted global warming, Global Biogeochem. Cy., 17, 2003.

Moore, J. K. and Doney, S. C.: Iron availability limits the ocean nitrogen inventory stabilizing feedbacks between marine denitrification and nitrogen fixation, Global Biogeochem. Cy., 21, GB2001, 2007.

Najjar, R. G., Jin, X., Louanchi, F., Aumont, O., Caldeira, K., Doney, S. C., Dutay, J.-C., Follows, M., Gruber, N., Joos, F., Lindsay, K., Maier-Reimer, E., Matear, R., Matsumoto, K., Monfray, P., Mouchet, A., Orr, J. C., Plattner, G.-K., Sarmiento, J. L., Schlitzer, R., Slater, R. D., Weirig, M.-F., Yamanaka, Y., and Yool, A.: Impact of circulation on export production, dissolved organic matter and dissolved oxygen in the ocean: Results from Phase II of the Ocean Carbon-cycle Model Intercomparison Project (OCMIP-2), Global Biogeochem. Cy., 21, 2007.

Parekh, P., Follows, M. J., and Boyle, E. A.: Decoupling of iron and phosphate in the global ocean, Global Biogeochem. Cy., 19, 2005.

Paulmier, A., Kriest, I., and Oschlies, A.: Stoichiometries of remineralisation and denitrification in global biogeochemical ocean model, Biogeosciences, 6, 923–935, 2009.

Piwonski, J. and Slawig, T.: Metos3D: the Marine Ecosystem Toolkit for Optimization and Simulation in 3-D – Part 1: Simulation Package v0.3.2, Geosci. Model Dev., 9, 3729–3750, doi:10.5194/gmd-9-3729-2016, www.geosci-model-dev.net/9/3729/2016/, 2016.

Priess, M., Koziel, S., and Slawig, T.: Marine ecosystem model calibration with real data using enhanced surrogate-based optimization, Journal of Computational Science, 4, 423–437, 2013.

Primeau, F. and Deleersnijder, E.: On the time to tracer equilibrium in the global ocean, Ocean Sci., 5, 13–28, 2009.

Raimbault, P., Garcia, N., and Cerutti, F.: Distribution of inorganic and organic nutrients in the South Pacific Ocean - evidence for long-term accumulation of organic matter in nitrogen-depleted waters, Biogeosciences, 5, 281–298, 2008.

Schartau, M., Wallhead, P., Hemmings, J., Löptien, U., Kriest, I., Krishna, S., Ward, B., Slawig, T., and Oschlies, A.: Reviews and syntheses: Parameter identification in marine planktonic ecosystem modelling, Biogeosciences Disc., doi:10.5194/bg-2016-242, 2016.

Schmoker, C., Hernandez-Leon, S., and Calbet, A.: Microzooplankton grazing in the oceans: impacts, data variability, knowledge gaps and future directions, Jour. Plank. Res., 35, 691–706, 2013.

Seferian, R., Gehlen, M., Bopp, L., Resplandy, L., Orr, J., Marti, O., Dunne, J. P., Christian, J., Doney, S., Ilyina, T., Lindsay, K., Halloran, P., Heinze, C., Segschneider, J., Tjiputra, J., Aumont, O., and Romanou, A.: Inconsistent strategies to spin up models in CMIP5: implications for ocean biogeochemical model performance assessment, Geosci. Model Dev., 9, 1827—1851, doi:10.5194/gmd-9-1827-2016, www. geosci-model-dev.net/9/1827/2016/, 2016.

Shimoda, Y. and Arhonditsis, G.: Phytoplankton functional type modelling: Running before we can walk? A critical evaluation of the current state of knowledge, Ecological Modelling, 320, 29–43, doi:10.1016/j.ecolmodel.2015.08.029, 2016.

Siberlin, C. and Wunsch, C.: Oceanic tracer and proxy time scales revisited, Clim. Past, 7, 27–39, 2011.

Torres-Valdes, S., Roussenov, V., Sanders, R., Reynolds, S., Pan, X., Mather, R., Landolfi, A., Wolff, G., Achterberg, E., and Williams, R.: Distribution of dissolved organic nutrients and their effect on export production over the Atlantic Ocean Distribution of dissolved organic nutrients and their effect on export production over the Atlantic Ocean, Glob. Biogeochem. Cyc., 23, doi:10.1029/2008GB003389, 2009.

Van Mooy, B., Keil, R., and Devol, A.: Impact of suboxia on sinking particulate organic carbon: Enhanced carbon flux and preferential degradation of amino acids via denitrificiation, Geochim. Cosmochim. Ac., 66, 457–465, 2002.

Wallmann, K.: Phosphorus imbalance in the global ocean?, Global Biogeochem. Cy., 24, 2010.

Ward, B., Friedrichs, M. A. M., Anderson, T., and Oschlies, A.: Parameter optimisation techniques and the problem of underdetermination in marine biogeochemical models, Jour. Mar. Systems, 81, 34–43, 2010.

Wunsch, C. and Heimbach, P.: How long to oceanic tracer and proxy equilibrium?, Quaternary Science Reviews, 27, 637–651, 2008.

Yool, A., Popova, E. E., and Anderson, T. R.: MEDUSA-1.0: a new intermediate complexity plankton ecosystem model for the global domain, Geosci. Model Dev., 4, 381–417, 2011.

Yoshimura, T., Nishioka, J., Saito, H., Takeda, S., Tsuda, A., and Wells, M. L.: Distributions of particulate and dissolved organic and inorganic phosphorus in North Pacific surface waters, Mar. Chem., 103, 112–121, 2007.

Table 1. Experimental setup of optimisation. Parameters that stay fixed are highlighted. For parameters to be optimised we indicate the lower and upper parameter boundary (parameter range, R_Θ^A) for optimisation in square brackets. "-": not applicable for this model.

Experiment	MOPS^r	MOPS^{oS}	MOPS^{oD}	RetroMOPS^r	RetroMOPS^o	unit
σ_{DOP}	-	-	-	**0.67**	[0.4 - 0.8]	
λ_{sDOP}	-	-	-	**0**	[0.0 - 3.6]	y^{-1}
λ_{DOP}	**0.17**	**0.17**	**0.17**	**0.36**	[0.036 - 3.6]	y^{-1}
I_c	**24**	[4 - 48]	**9.65**	**9.65**	**9.65**	W m^{-2}
K_{PHY}	**0.03125**	[0.001 - 0.5]	**0.5**	**0.5**	**0.5**	mmol P m^{-3}
μ_{ZOO}	**2**	[1 - 3]	**1.89**	-	-	d^{-1}
κ_{ZOO}	**3.2**	[1.6 - 4.8]	**4.55**	-	-	(d mmol P m^{-3})$^{-1}$
b^*	**0.858**	[0.4 - 1.8]	[0.4 - 1.8]	**1.0725**	[0.4 - 1.8]	
$R_{-O2:P}$	**170**	[150 - 200]	[150 - 200]	**171.7**	**171.7**	mmol O$_2$:mmol P
μ_{NFix}	**2**	**2**	[1 - 3]	**1.19**	**1.19**	nmol N d^{-1}
DIN_{min}	**4**	**4**	[1 - 16]	**15.79**	**15.80**	mmol N m^{-3}
K_{O2}	**2**	**2**	[1 - 16]	**1.0**	**1.0**	mmol O$_2$ m^{-3}
K_{DIN}	**8**	**8**	[2 - 32]	**31.97**	**31.97**	mmol N m^{-3}

* Note that from b (the optimised parameter) in MOPS we calculate the rate of vertical increase in sinking speed a of $w = a\,z$, via $a = r/b$. For r we assume nominal detrital remineralisation of $r = 0.05$ d^{-1}. The resulting values for a are: 0.058275 ($b = 0.858$), 0.0278 (lower boundary) and 0.125 (upper boundary).

Table 2. Results (misfit J) of sensitivity experiments with model RetroMOPS, regarding parameters λ_{sDOP} and λ_{DOP} for DOP decay rate. The misfit of the reference scenario RetroMOPS^r is indicated in bold.

	$\lambda_{sDOP} = 0$	$\lambda_{sDOP} = 0.18$	$\lambda_{sDOP} = 0.36$
$\lambda_{DOP} = 0.18$	0.502	0.480	0.480
$\lambda_{DOP} = 0.36$	**0.466**	0.476	0.493
$\lambda_{DOP} = 0.72$	0.503	0.522	0.539

Table 3. Optimisation results: minimum misfit J^*, optimum parameters and their uncertainties. To determine parameter uncertainty, we selected a group Ω of the 1‰ best individuals, i.e. individuals defined by a misfit $J_i : J_i/J^* - 1 \leq \Delta_J$, with $\Delta_J = 0.001$. The number of these individuals $N(\Omega)$ is also denoted as fraction $n(\Omega)$ of all individuals of the optimisation $\lambda \times N$, where N is the number of generations, and $\lambda = 10$ the population size. For each parameter Θ the first column gives the optimal parameter Θ^* (i.e., the average parameter of the last generation). The second and third column present the parameter range of all individuals of Ω, expressed as absolute value ($R_\Theta(\Omega)$), and normalised by the a priori range of parameters (R_Θ^A; see Table 1): $r_\Theta(\Omega) = R_\Theta(\Omega)/R_\Theta^A$ value.

Experiment:	MOPS^{oS}			MOPS^{oD}			MOPS$_*^{oD}$			RetroMOPS^o		
Parameter	Θ^*	$R_\Theta(\Omega)$	$r_\Theta(\Omega)$	Θ^*	$R_\Theta(\Omega)$	$r_\Theta(\Omega)$	Θ^*	$R_\Theta(\Omega)$	$r_\Theta(\Omega)$	Θ^*	$R_\Theta(\Omega)$	$r_\Theta(\Omega)$
σ_{DOP}	-	-	-	-	-	-	-	-	-	0.73	[0.7-0.7]	6
λ_{sDOP}	-	-	-	-	-	-	-	-	-	0.02	[-0.1-0.2]	8
λ_{DOP}	-	-	-	-	-	-	-	-	-	0.47	[0.4-0.5]	4
I_c	9.66	[8.9-10.3]	3									
K_{PHY}	0.50	[0.4-0.5]	28									
μ_{ZOO}	1.89	[1.6-2.0]	22							-	-	-
κ_{ZOO}	4.57	[3.0-4.7]	53							-	-	-
$b^\S$	1.34	[1.3-1.4]	4	1.39	[1.4-1.4]	3	1.41	[1.4-1.4]	2	0.98	[1.0-1.0]	2
$R_{-O2:P}$	167.0	[165-170]	9	171.7	[170-173]	6	174.9	[174-176]	5			
μ_{NFix}				1.19	[1.1-1.4]	13	1.47	[1.4-1.6]	10			
DIN_{min}				15.80	[13-16]	20	12.96	[12-16]	25			
K_{O2}				1.00	[0.3-1.8]	10	1.00	[0.5-1.4]	6			
K_{DIN}				31.97	[30-34]	12	31.97	[22-33]	35			
J^*	0.450			0.439			0.427			0.458		
$\lambda \times N$	1820			1190			2000			660		
$N(\Omega)$	718			514			1285			262		
$n(\Omega)$	39			43			64			40		

Table 4. Global annual fluxes of primary production (P), grazing (GRAZ), fixed nitrogen loss through pelagic denitrification (NLOSS), export production (F120, flux through 120 m), flux through 2250 m (F2250), and benthic burial (BUR), in Pg N y^{-1}, for the reference experiment of MOPS^{r}, MOPS^{oS}, MOPS^{oD}, MOPS$_*^{oD}$ and RetroMOPS, for which we show the fluxes of the (best) reference experiment, RetroMOPS^{r}, the range of all sensitivity experiments, and the optimised run, RetroMOPS^{o}. Also shown are some globally derived, observed estimates. Conversion between different elements was carried out via N:P=16, and C:P=122.

Experiment	P	GRAZ	NLOSS	F120	F2250	BUR
MOPS^{r}	5.44	3.52	0.098	0.918	0.107	0.051
MOPS^{oS}	7.52	4.74	0.117	1.102	0.056	0.018
MOPS^{oD}	7.70	4.97	0.068	1.080	0.055	0.022
MOPS$_*^{oD}$	7.80	5.06	0.083	1.081	0.053	0.021
RetroMOPS^{r}	5.56	-	0.078	1.194	0.043	0.010
RetroMOPS (range)	4.88-6.21	-	0.076-0.084	1.076-1.286	0.039-0.047	0.008-0.014
RetroMOPS^{o}	6.31	-	0.071	1.12	0.052	0.009
Observed[§]	7.68-8.09	4.79-5.71	0.05-0.08	0.29-1.53	0.03-0.07	0.02

[§] Observed fluxes are from Carr et al. (2006, primary production), Honjo et al. (2008, particle flux), Lutz et al. (2007, particle flux), Dunne et al. (2007, particle flux), Schmoker et al. (2013, primary production, zooplankton grazing excluding/including mesozooplankton grazing), Wallmann (2010, burial; without shelf and slope region), and Kriest and Oschlies (2015, fixed nitrogen loss).
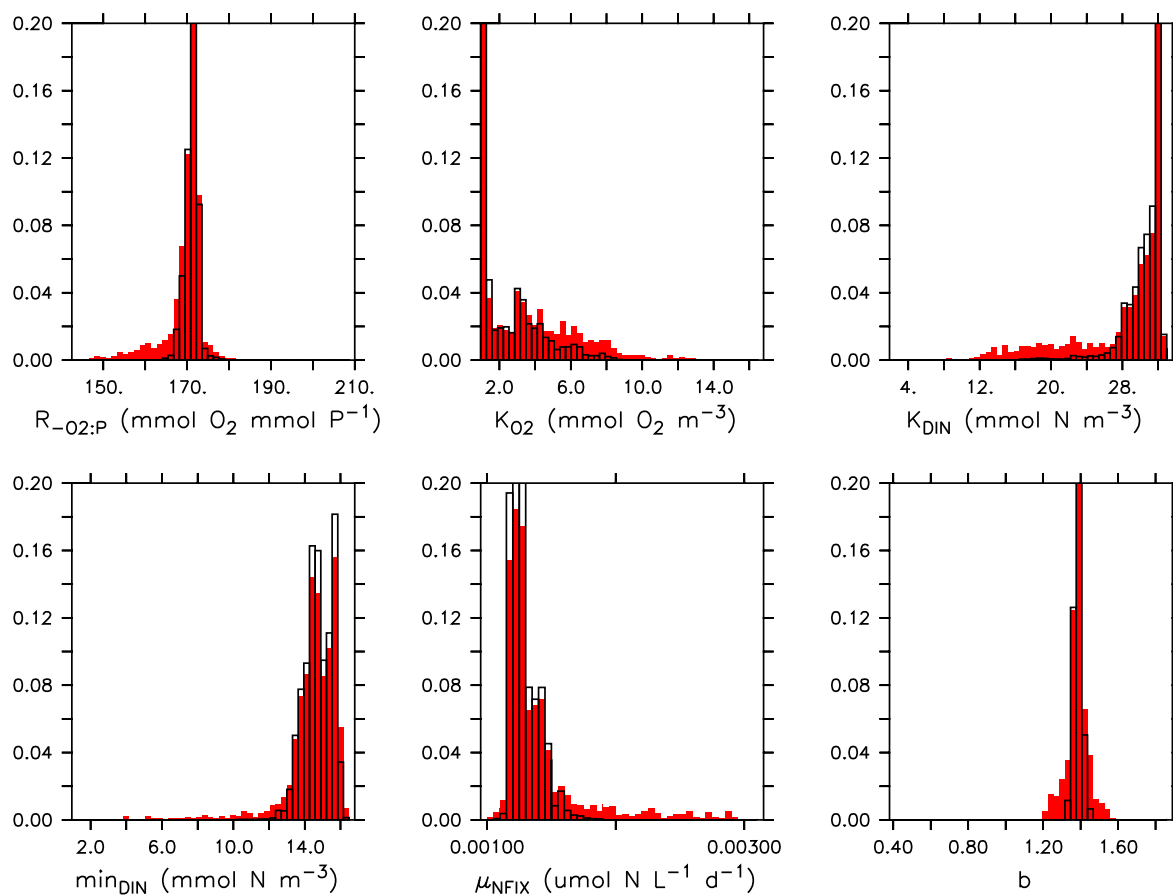
Figure 1. Parameter distribution of model simulations obtained during the optimisation of $MOPS^{oD}$, whose misfit do not exceed a threshold limit of $\Delta J = 1.1\,J^{*}$ (10%, red bars) or $\Delta J = 1.01\,J^{*}$ (1%, open bars) of the minimum misfit J^{*}. For the projection parameters of all model simulations in the optimisation trajectory were grouped into 50 classes.
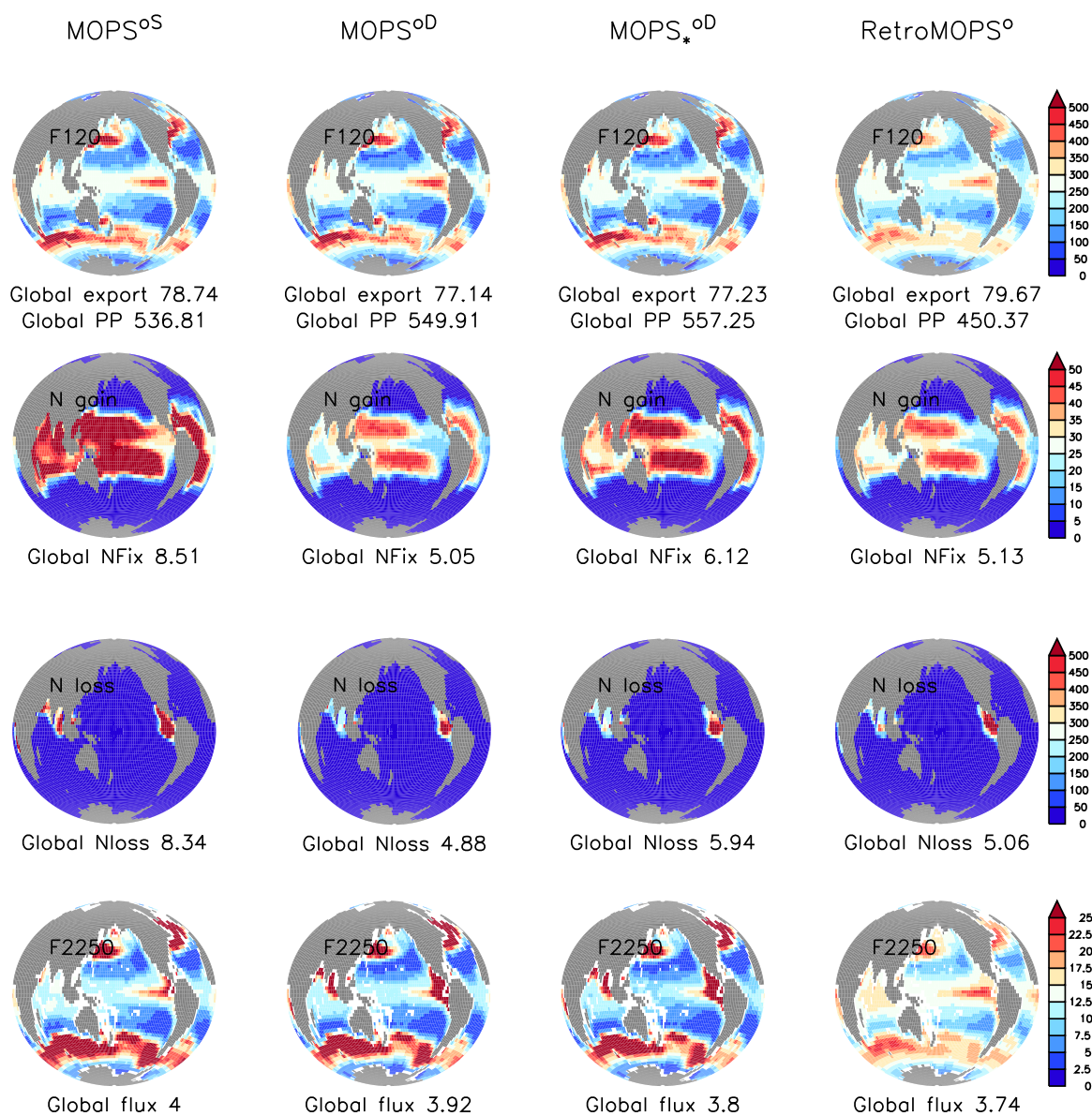
Figure 2. Biogeochemical fluxes of MOPS^{oS}, MOPS^{oD}, MOPS$_*^{oD}$ and RetroMOPS^o. Top: Export production (here: sedimentation at 120 m). Second row from top: nitrogen fixation. Third row from top: fixed nitrogen loss through pelagic denitrification. Bottom: sedimentation at 2250 m. All fluxes in mmol N m^{-2} y^{-1}. Each subpanel also gives the global flux in Tmol N y^{-1}.
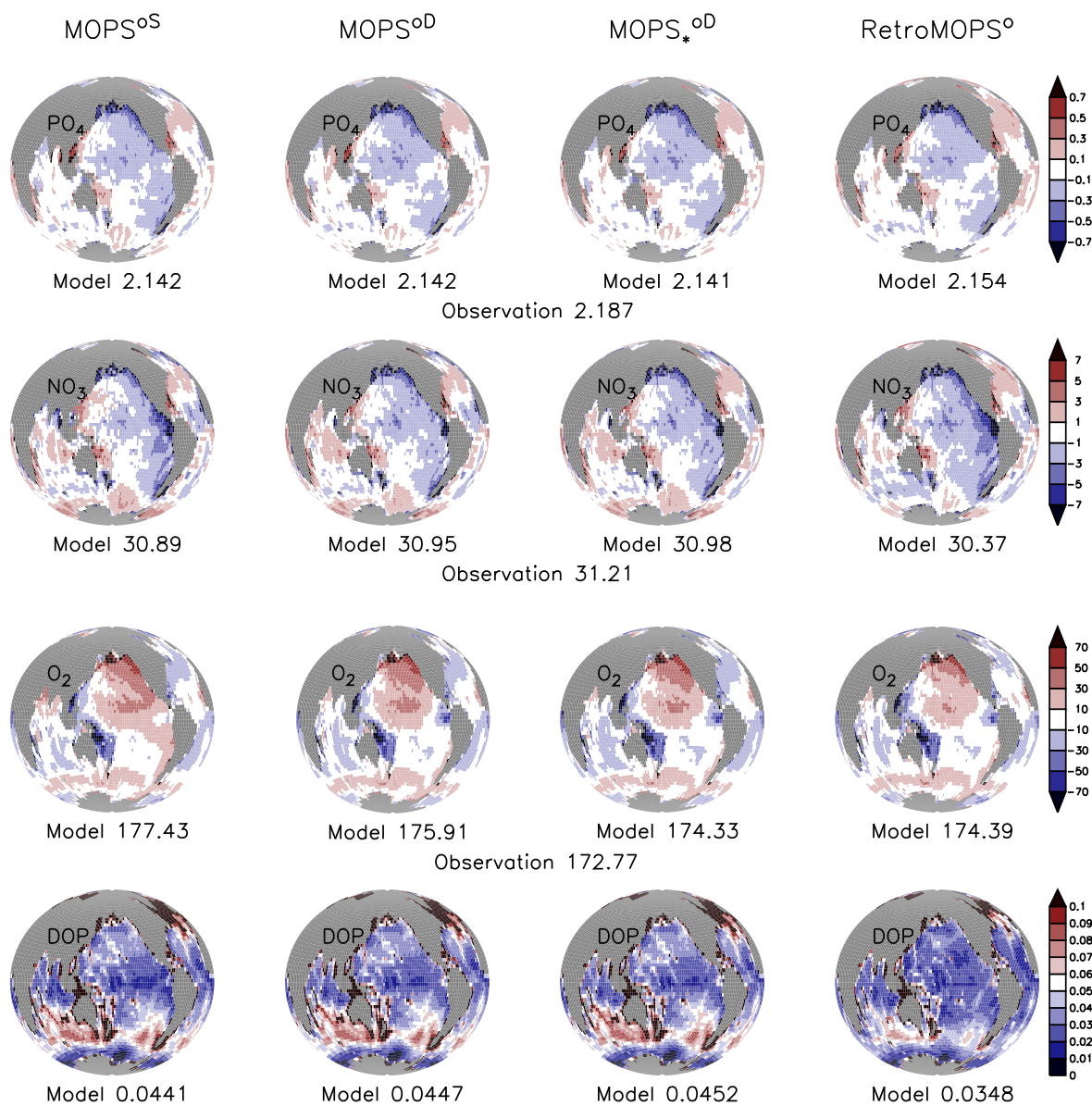
Figure 3. Vertically averaged tracers of MOPS[oS], MOPS[oD], MOPS[oD]$_*$ and RetroMOPS[o]. Top: phosphate. Second row from top: nitrate. Third row from top: oxygen. Bottom: DOP. Phosphate (mmol P m^{-3}), nitrate (mmol N m^{-3}) and oxygen (mmol O$_2$ m^{-3}) are expressed as deviation from observations (Garcia et al., 2006a, b), DOP is given in absolute concentrations (mmol P m^{-3}). Each subpanel also gives the global average tracer concentration in mmol m^{-3}.
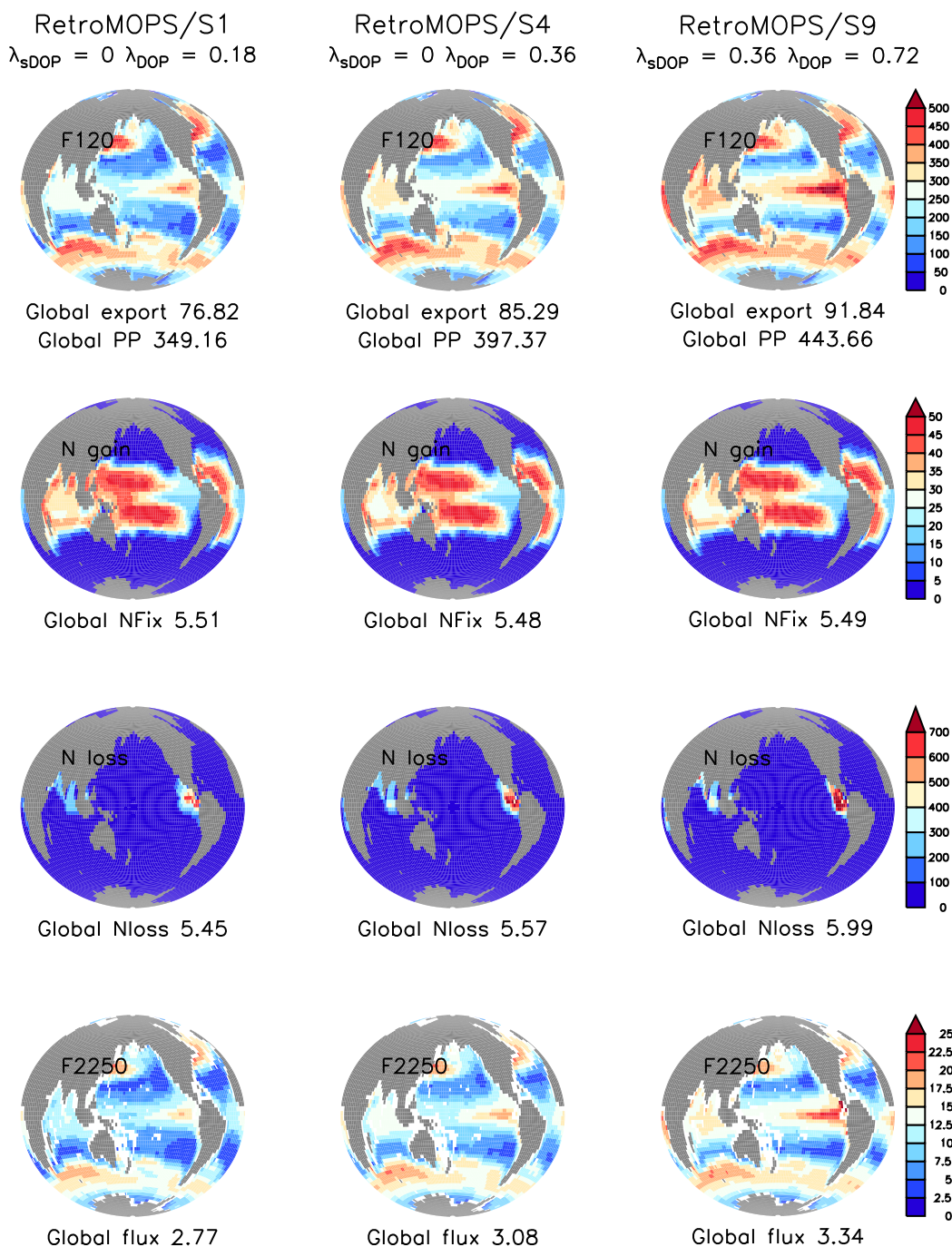
Figure 4. As Fig. 2, but for three sensitivity experiments with model RetroMOPS.
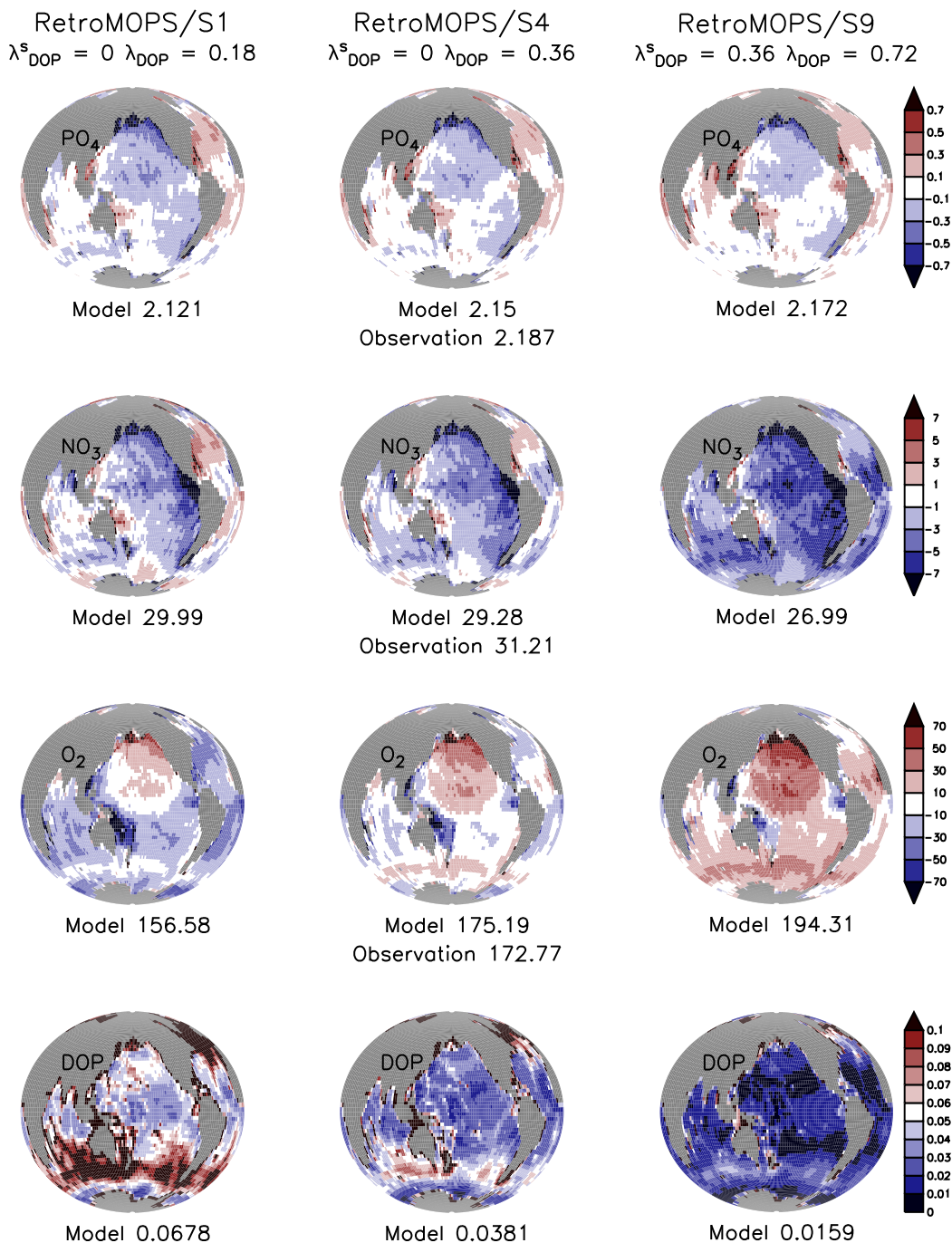
Figure 5. As Fig. 3, but for three sensitivity experiments with model RetroMOPS.
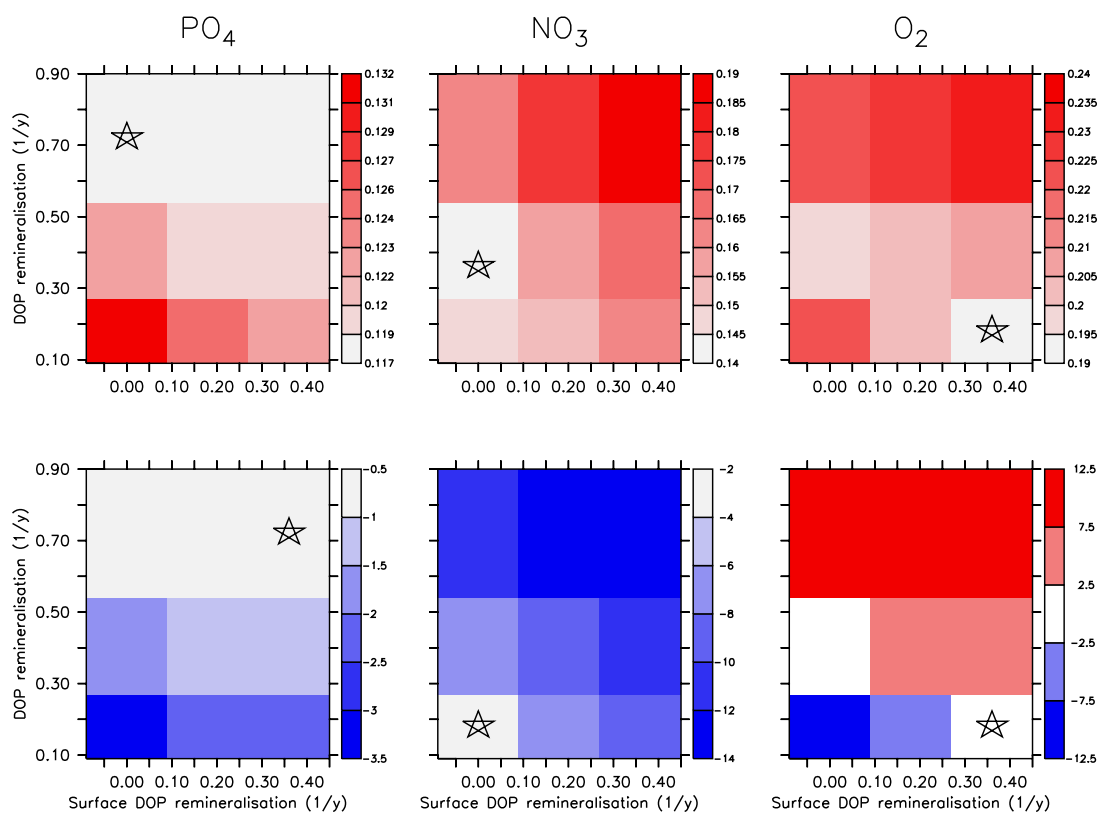
Figure 6. Components of the misfit function ($J(j)$ of Eqn. 11; upper panels) and model bias (lower panels), projected onto λ_{sDOP} and λ_{DOP}. Bias is expressed as $(\overline{m_j}/\overline{o_j} - 1) \times 100$, where $\overline{m_j}$ is the global average model tracer, and $\overline{o_j}$ the average observed tracer, for the three tracers phosphate ($j = 1$; left panels), nitrate ($j = 2$; mid panels) and oxygen ($j = 3$; right panels). An open star indicates the respective lowest misfit or bias.
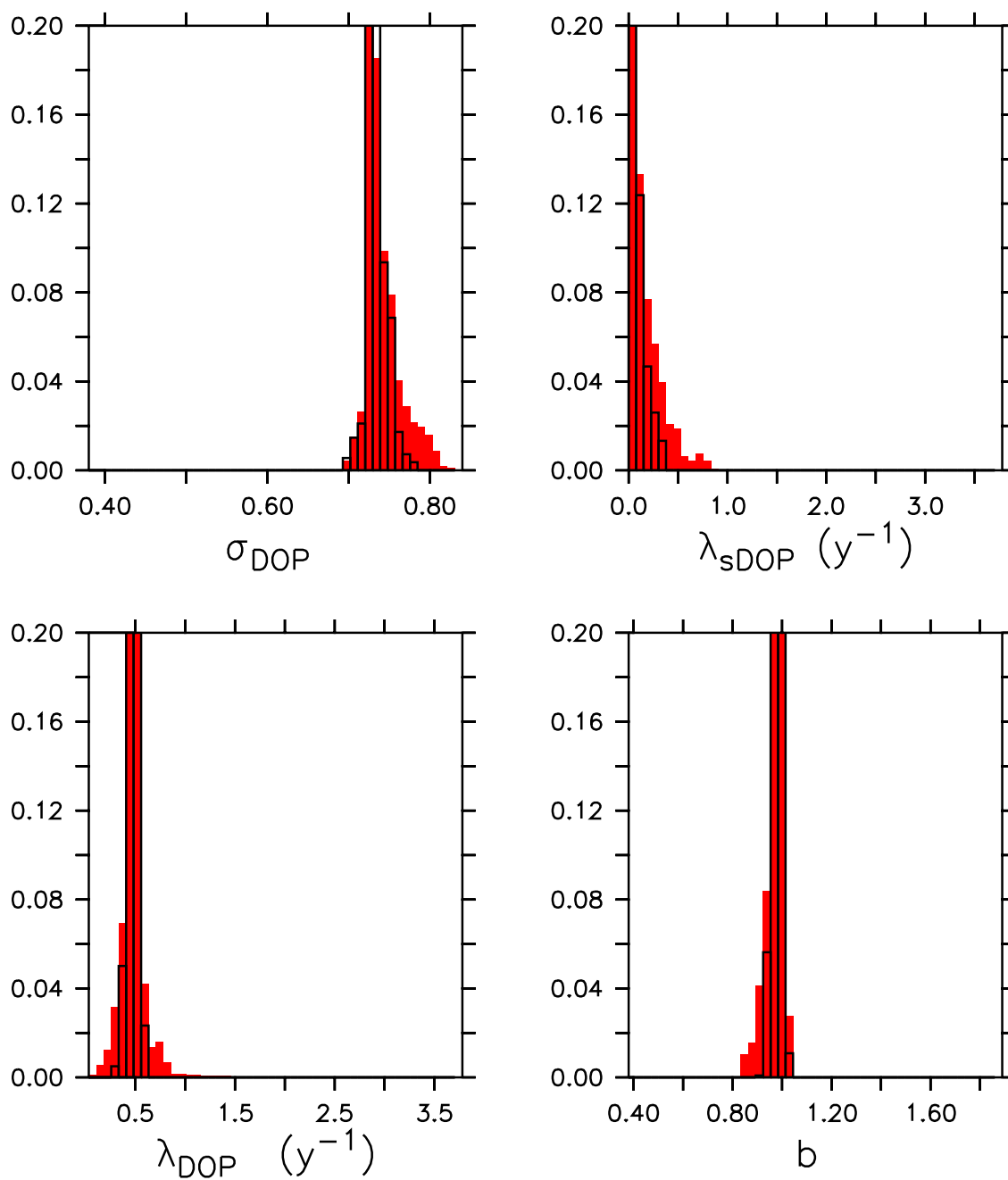
Figure 7. As Fig. 1, but for optimisation RetroMOPS°.
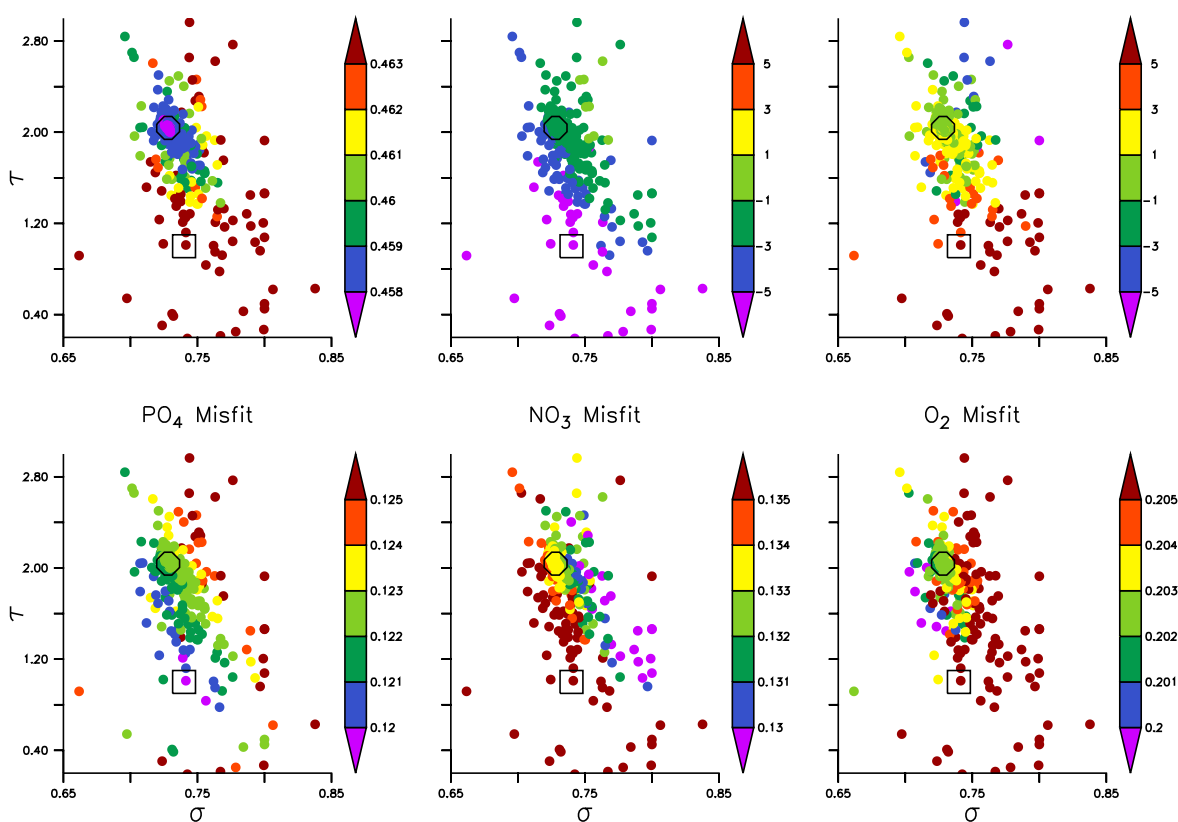
Figure 8. Model misfit and relative bias b_j of RetroMOPS°, plotted for parameter combinations of σ_{DOP} and DOP decay timescale τ, where $\tau = 1/(\lambda_{\mathrm{DOP}} + \lambda_{\mathrm{sDOP}})$. Relative bias is evaluated by $b_j = (\overline{m_j}/\overline{o_j} - 1) \times 100$, where $\overline{m_j}$ denotes the global mean model concentration of tracer j, and $\overline{o_j}$ the observed mean. Model misfit is shown as total misfit (J of Eqn. 11; upper left), and seperated into it components, normalised by $\overline{o_j}$ ($J(j)$ of Eqn. 11; lower panels). The analysis is restricted to all individuals i whose b differs less than 5% from optimal b^*, i.e. $|b_i/b^* - 1| < 0.05$. For better visibility some model solutions (≈ 10), that are outside the range $0.65 \leq \sigma \leq 0.85$ and $0.2 \leq \tau \leq 3$ have been ommitted from the plot. Open squares denote optimal estimates by Kwon and Primeau (2006, total phosphate constraint), open circles the optimal parameter from this study.